



RESEARCH ARTICLE

10.1029/2023SW003687

Key Points:

- Geomagnetic disturbances induce electric fields in both the sea and in submarine cables
- Earth potentials are produced by the geoelectric coast effect at each end of a cable route
- Voltages experienced by submarine cables are due to both the induced electric fields and earth potentials at the ends

Supporting Information:

Supporting Information may be found in the online version of this article.

Correspondence to:

D. H. Boteler,
david.boteler@nrcan-rncan.gc.ca

Citation:

Boteler, D. H., Chakraborty, S., Shi, X., Hartinger, M. D., & Wang, X. (2024). An examination of geomagnetic induction in submarine cables. *Space Weather*, 22, e2023SW003687. <https://doi.org/10.1029/2023SW003687>






Received 20 AUG 2023

Accepted 31 OCT 2023

Author Contributions:

Conceptualization: David H. Boteler
Investigation: David H. Boteler, Shibaji Chakraborty, Xueling Shi, Michael D. Hartinger, Xuan Wang
Methodology: David H. Boteler, Shibaji Chakraborty, Xuan Wang
Software: Shibaji Chakraborty
Supervision: David H. Boteler
Visualization: Shibaji Chakraborty
Writing – original draft: David H. Boteler

An Examination of Geomagnetic Induction in Submarine Cables

David H. Boteler¹ , Shibaji Chakraborty² , Xueling Shi^{2,3} , Michael D. Hartinger⁴ , and Xuan Wang⁵ 

¹Geomagnetic Laboratory, Natural Resources Canada, Ottawa, ON, Canada, ²Center for Space Science and Engineering Research, Virginia Tech, Blacksburg, VA, USA, ³High Altitude Observatory, National Center for Atmospheric Research, Boulder, CO, USA, ⁴Space Science Institute, Boulder, CO, USA, ⁵Department of Electrical Engineering, Tsinghua University, Beijing, China

Abstract Submarine cables have experienced problems during extreme geomagnetic disturbances because of geomagnetically induced voltages adding or subtracting from the power feed to the repeaters. This is still a concern for modern fiber-optic cables because they contain a copper conductor to carry power to the repeaters. This paper provides a new examination of geomagnetic induction in submarine cables and makes calculations of the voltages experienced by the TAT-8 trans-Atlantic submarine cable during the March 1989 magnetic storm. It is shown that the cable itself experiences an induced electromotive force (emf) and that induction in the ocean also leads to changes of potential of the land at each end of the cable. The process for calculating the electric fields induced in the sea and in the cable from knowledge of the seawater depth and conductivity and subsea conductivity is explained. The cable route is divided into 9 sections and the seafloor electric field is calculated for each section. These are combined to give the total induced emf in the cable. In addition, induction in the seawater and leakage of induced currents through the underlying resistive layers are modeled using a transmission line model of the ocean and underlying layers to determine the change in Earth potentials at the cable ends. The induced emf in the cable and the end potentials are then combined to give the total voltage change experienced by the cable power feed equipment. This gives results very close to those recorded on the TAT-8 cable in March 1989.

Plain Language Summary Submarine cables carry a significant amount of international internet traffic, so any disruption to their operation could have widespread consequences. In the past, trans-Atlantic phone calls have been heard alternately as shrieks and whispers as geomagnetically induced voltages added or subtracted from the power feed for the cable repeaters used to amplify the signals. Modern submarine cables transmit the signals along optical fibers but still have a copper conductor along the cable to carry power to the repeaters, so continue to be subject to voltages induced by disturbances of the Earth's magnetic field. This paper re-examines the process of geomagnetic induction in the sea and submarine cables. It is shown that this involves both the production of an induced electromotive force (emf) in the cable itself as well as induction in the seawater that leads to a change in the potential of the land at each end of the cable. Example calculations are made for the TAT-8 trans-Atlantic cable and compared to measurements made on the cable during 13 and 14 March 1989, the largest magnetic storm of the 20th century.

1. Introduction

During geomagnetic disturbances, the variations of the Earth's magnetic field induce electric currents in the Earth and in human-made conductors at, or under, the Earth's surface. Communications cables, power systems, pipelines, and railway signaling can be disrupted during extreme disturbances (Boteler et al., 1998). During the Carrington event of 1859, the telegraph system suffered widespread problems from geomagnetic induction (Boteler, 2006; Prescott, 1866). Later disturbances continued to cause problems for the telegraph system and for submarine cables (see review by Burbank (1905) and references therein). The development in the 1950s of cables with repeaters powered by a current fed along the cable introduced a new vulnerability. Telephone calls over the first trans-Atlantic phone cable, TAT-1, alternated between loud squawks and faint whispers as the naturally induced voltage acted with or against the cable supply voltage during the magnetic storm of 10 February 1958 (Anderson, 1978). Cables on land could also be affected: a section of the L4 cross-continental cable system was put out of operation during the August 1972 storm (Anderson et al., 1974). Fiber-optic cables were introduced in

© 2024 His Majesty the King in Right of Canada and The Authors. Reproduced with the permission of the Minister of Natural Resources Canada. This is an open access article under the terms of the [Creative Commons Attribution-NonCommercial-NoDerivs License](https://creativecommons.org/licenses/by-nc-nd/4.0/), which permits use and distribution in any medium, provided the original work is properly cited, the use is non-commercial and no modifications or adaptations are made.

Writing – review & editing: David H. Boteler, Shibaji Chakraborty, Xueling Shi, Michael D. Hartinger, Xuan Wang

the 1980s, and transmit the signal along optical fibers, while maintaining copper conductors to carry power to the repeaters. Geomagnetic disturbances may still affect the power feed to these cables, as shown by recordings made on the TAT-8 cable during the March 1989 storm. Thus, the effects of geomagnetic disturbances on submarine cables are still a cause for concern.

The understanding of geomagnetically induced currents (GIC)—also referred to as “Earth currents” and “telluric currents”—has evolved substantially over the last 150 years. Often, it was the concerns about their impacts on technological systems that were a stimulus for research into the currents themselves. Lanzerotti and Gregori (1986) provide a good review of the historical development of the understanding of telluric currents and an assessment of their effects on communication cables and other systems. In the 19th century there was still debate about the cause of magnetic disturbances and whether they were produced by electric currents in the Earth. Over the years it came to be recognised that geomagnetic disturbances are caused by electric currents external to the Earth, and that earth currents are the result of geomagnetic induction. However, there has been confusion about the nature of the electric fields driving the induced currents and the location of return currents. Winckler et al. (1959) report on the submarine cable voltage fluctuations seen during the February 1958 disturbance and try to relate them to induction in a loop in the vertical plane or in the horizontal plane. Later studies of the diurnal variation of cable voltages due to the Sq magnetic field variation (Medford et al., 1981) attempt to estimate the area influenced by the induction process. Some authors described the voltages observed in submarine cables as caused by changes in the magnetic field, while others believed that the voltage is caused by a difference in the potentials at the ends of the cable. This confusion has hindered the understanding of geomagnetic induction in submarine cables.

Developments in geophysics and engineering have produced new knowledge that can be applied to submarine cable questions. A significant advance was made with the work of Tikhonov (1950) and Cagniard (1953) that showed the relationship between the electric field and magnetic field variations and the earth conductivity, leading to the “magnetotelluric” technique. Associated theoretical work by Wait (1954, 1962) and Price (1962) provided the mathematical foundation for understanding the basic relationships between electric and magnetic fields. Later reviews by Bullard and Parker (1970) and Cox et al. (1970), specifically focus on induction in the sea. Early modeling of GIC in power systems represented the driving force as potential gradients at the Earth's surface, but it was later shown that GIC are driven by induced electromotive forces (emfs) in the power transmission lines (Boteler & Pirjola, 1998; also see review by Boteler & Pirjola, 2017). Boteler and Pirjola (1997), examined the nature of the electric fields associated with GIC and showed that they can be resolved into scalar potential and vector potential terms that can be uniquely associated with different sources: the distribution of charge and the fluctuation of the magnetic field. The geoelectric field affecting long conductors is primarily induced by magnetic field changes, while potential gradients are secondary effects caused by charge accumulation at conductivity boundaries.

The purpose of this paper is to re-examine the issue of geomagnetic induction in submarine cables, taking into account the knowledge derived from magnetotelluric studies and studies of GIC in power systems. First, we consider a number of fundamental issues about the induction process. Next, we present the theory for calculating the voltages experienced by submarine cables during geomagnetic disturbances. The application of this theory is illustrated by calculating the voltages experienced by the TAT-8 trans-Atlantic cable during the March 1989 magnetic storm and comparing them to the voltages observed on the cable.

2. Fundamental Issues

2.1. Induction in a Loop

Faraday's law (the integral form of Maxwell's equation) provides the relationship between the voltage induced in a loop and the rate of change of the magnetic flux through the loop. Consequently, many studies of geomagnetic induction in technological systems have attempted to use this relationship to calculate the voltages produced. For power systems, the obvious loop to consider is that formed by the power line and the Earth's surface; however, the voltages calculated with this loop are too small to account for the geomagnetically induced currents observed (Boteler & Pirjola, 2017). For submarine cables, the situation is more complicated with possible return paths through the sea above the cable or through the Earth below the seafloor. Winckler et al. (1959) considered these options and reported that neither is satisfactory.

To understand how the concept of “induction in a loop” can be applied to geomagnetic induction we need to consider the fall-off of the magnetic field variations within the Earth. If we approximate the Earth by a half-space

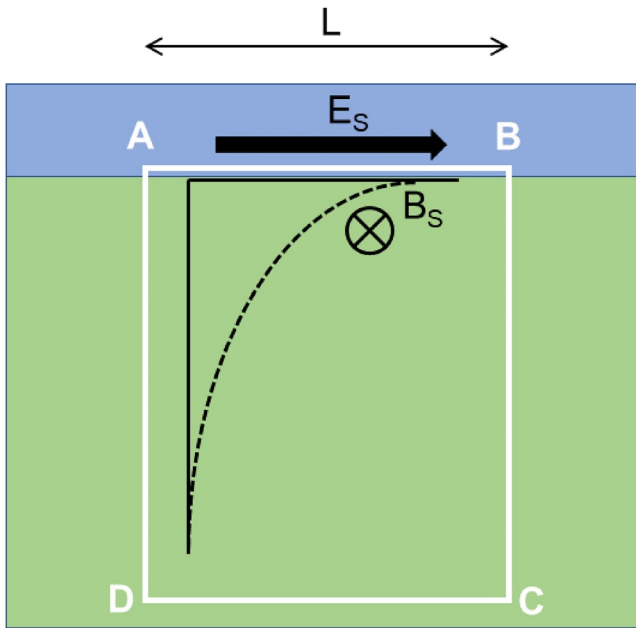


Figure 1. Geomagnetic induction in the loop ABCD where sides AB and CD have length L and sides AD and BC are infinite. The blue and green sections represent sea water layer and the Earth below the sea water layer. The dashed black line shows the fall-off within the Earth of the northward magnetic field (B_s , is into the page) variations that are responsible for inducing an east-west directed electric field (E_s).

with uniform conductivity, σ , and consider an incident magnetic field varying with a frequency, f , the decrease of the magnetic field with increasing depth, z , is given by

$$B(z) = B_0 e^{-kz} \quad (1)$$

where k is the propagation constant given by

$$k = \sqrt{i2\pi f \mu_0 \sigma} \quad (2)$$

and μ_0 is the magnetic permeability which is given its free space value $4\pi \cdot 10^{-7}$ H/m. The propagation constant can be written in terms of real and imaginary parts, $k = a + ib$ where a is the attenuation constant and b is the phase constant. From this we can define the skin depth, δ

$$\delta = \frac{1}{a} = \sqrt{\frac{1}{\pi f \mu_0 \sigma}} \quad (3)$$

and the wavelength in the Earth

$$\frac{\lambda}{2\pi} = \frac{1}{b} = \sqrt{\frac{1}{\pi f \mu_0 \sigma}} \quad (4)$$

Comparing Equations 3 and 4 shows that the skin depth in the Earth is less than a sixth of a wavelength. Thus, nearly all the induced current is concentrated near the surface and is flowing in the same direction. At a depth where the current is flowing in the opposite direction, its amplitude is so small that its value is insignificant. This is consistent with the role of the induced currents in “shielding” the interior of the Earth from the incident magnetic field variations and shows that there is no “return current” at depth.

Instead, the induced currents flow in large horizontal loops that correspond to image currents below the ionospheric current systems responsible for the magnetic disturbances.

Knowing the fall-off of the fields within the Earth below the seafloor allows us to calculate the seafloor electric fields. Consider an east-west section of the seafloor of length, L , as shown in Figure 1 with a northward magnetic field variation producing an eastward electric field at the seafloor, E_s . To calculate the seafloor electric field, we can consider the loop ABCD extending to infinity below the seafloor. The magnetic field through the loop ABCD is found by integrating Equation 1 for depths below the seafloor from 0 to infinity and multiplying by the length L :

$$\Phi = \int_0^\infty B(z) dz L = B_s p L \quad (5)$$

Where p is the complex skin depth given by $1/k$.

Using Faraday's law we can relate the electric field around the loop ABCD to the negative rate of change of the magnetic field, Φ through the loop

$$\oint_{ABCD} E dl = -\frac{d\Phi}{dt} = -j\omega B_s p L \quad (6)$$

where ω is the angular frequency of the magnetic field variation. The integral of the electric field around the loop ABCD is the sum of the electric fields along each side. For the side AB the integrated electric field is the seafloor electric field, E_s , times the length, L . The electric field is horizontal, so the electric field along the vertical sides of the loop, BC and DA, will be zero. The side of the loop CD is at infinity where the fields have decayed to zero so the electric field here is also zero. Thus, the integral of the electric fields around the loop ABCD is simply given by $E_s L$. Substituting this into Equation 6 and dividing by L gives the seafloor electric field

$$E_s = -j\omega B_s p \quad (7)$$

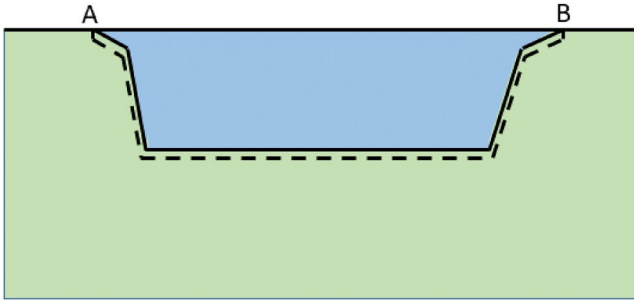


Figure 2. Schematic of a submarine cable connecting the opposite sides of an ocean. The solid line shows the path A to B through the copper conductor in the cable and the dashed line shows the return path B to A along the seafloor next to the cable.

Thus, induction in a loop can be used to calculate the electric fields at the surface of the Earth or at the seafloor as long as the proper loop is taken into account. This is equivalent to the result achieved using the relationship between the electric and magnetic fields in terms of the surface impedance (Boteler & Pirjola, 2017). This has been extended to calculate the seafloor electric fields for a layered subsea conductivity structure and using the magnetic fields at the ocean surface (Boteler & Pirjola, 2003).

2.2. Geomagnetic Induction in Submarine Cables

The above section has shown that we can calculate the electric fields at the seafloor. But we want to know the induced electric fields experienced by a submarine cable itself. To do this, consider the closed loop formed by the path along the copper conductor of the cable and returning along the seafloor next to the cable as shown in Figure 2.

From Faraday's law we know that the integral of the electric field, E , around the loop formed by the cable, C , and the seafloor, S , is equal to the negative rate of change of the magnetic flux through the loop:

$$\oint_{C+S} \vec{E} \cdot d\hat{l} = -\frac{d\Phi}{dt} \quad (8)$$

where, $\Phi = \iint_A \vec{B} \cdot d\hat{A}$, and A is the area enclosed by the loop formed by the cable and seafloor. However, because the cable and the return path along the seafloor are next to each other the area of the loop is effectively zero so there is no magnetic flux change through the loop. Therefore, we can write:

$$\int_A^B \vec{E}_C \cdot d\hat{l} + \int_B^A \vec{E}_S \cdot d\hat{l} = 0 \quad (9)$$

Where E_C is the electric field along the cable, E_S is the electric field along the seafloor, and the integrals go from A to B along the cable and back from B to A along the seafloor.

Reversing the direction of integration for the seafloor path then gives:

$$\int_A^B \vec{E}_C \cdot d\hat{l} = \int_A^B \vec{E}_S \cdot d\hat{l} \quad (10)$$

showing that the electric field along the cable is the same as the electric field along the seafloor next to the cable. This is the same approach described by Cox et al. (1970) for the electric fields detected by measuring equipment on the seafloor.

If we consider a cable running across an ocean from one end at the coast, A, to the other end at the coast, B. Then the total emf induced in the cable, \mathcal{E}_C is given by the integral of the electric field along the cable:

$$\mathcal{E}_C = \int_A^B \vec{E}_C \cdot d\hat{l} \quad (11)$$

that can be calculated from Equation 10.

2.3. Geoelectric Coast Effect

Electric fields produced during geomagnetic disturbances will drive electric currents in both the land and the ocean. The current densities in seawater will be much greater than those in the land and this leads to local modifications to the electric fields on either side of a coastline that are referred to as the "geoelectric coast effect."

To illustrate the processes that produce the geoelectric coast effect, Price (1973) considered a vertical boundary between two regions of different conductivity as shown in Figure 3. The conductivity of region 1, σ_1 , on the left side of the boundary is much greater than the conductivity of region 2, σ_2 , on the right side; this can be seen in

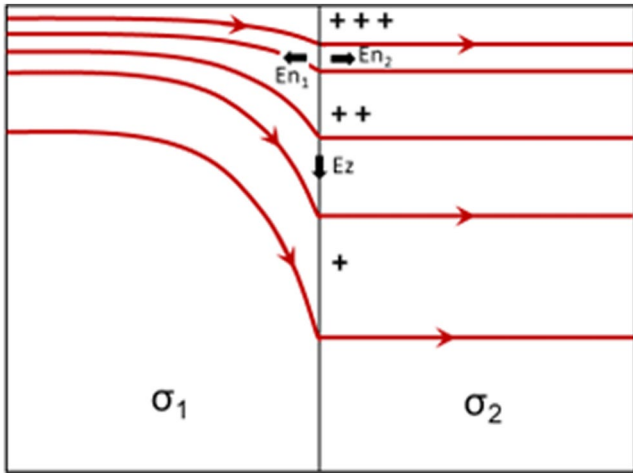


Figure 3. Current lines (red) and surface charge distribution (+) near a vertical plane of discontinuity between region 1 with conductivity, σ_1 , and region 2 with conductivity, σ_2 . The charges at the discontinuity create extra electric fields normal to the discontinuity, E_{n1} and E_{n2} and vertical electric field E_z that act to bend the currents down into the Earth and produce current continuity across the discontinuity (after Price, 1973).

the figure by the fact that the current flow lines are concentrated nearer the surface in region 1 where the higher conductivity results in a smaller skin depth. Current is a flow of charge, so a difference in current flowing into and out of the boundary region will result in an accumulation of charge at the boundary. This electrical charge creates an electric potential at the boundary and, in consequence, a potential gradient on either side. This potential gradient increases the electric field on the low conductivity side of the boundary and decreases the electric field on the higher conductivity side of the boundary. Thus, the initial difference in current density in the two regions produces the charge accumulation and changes to the electric fields that leads to current continuity across the boundary. The difference in current density decreases with depth so the amount of charge at the boundary also decreases with depth so, as well as the horizontal potential gradients, there is a vertical potential gradient that causes the currents near the surface in the higher conductivity region to divert downwards into the Earth as shown in Figure 3.

This geoelectric coast effect occurs at both ends of a submarine cable where the cable comes onshore to the cable station that houses the cable power feed equipment. The earth potentials at opposite ends of a cable will each act to reduce the electric current density on the seawater side of the coast and increase the current density on the land side. Thus, at each end of the cable route, the earth potentials will act to partially cancel the electric field in the seawater in the vicinity of the coast.

2.4. Voltage Affecting Power Feed for Submarine Cables

The power feed equipment at each end of the cable will be connected to local earth which, because of the geoelectric coast effect will have the potential, U_A , at the end of the cable, A, and potential, U_B , at the end of the cable, B. Thus, during geomagnetic disturbances, a submarine cable will experience a voltage, V_C , comprised of two parts: the induced electromotive force, \mathcal{E}_C , induced by the magnetic field variations directly in the cable and the potential difference between the ends of the cable

$$V_C = \mathcal{E}_C + U_A - U_B \quad (12)$$

Where: $\mathcal{E}_C = \oint_C \vec{E} \cdot d\hat{l}$ with the integration taken along the path of the cable,

U_A is the Earth potential at the end "A" of the cable,

U_B is the Earth potential at the end "B" of the cable.

3. Modeling of Geomagnetic Induction in Submarine Cables

To model the effects of geomagnetic induction on submarine cables we need to consider both the induced emf produced in the cable itself and the change in Earth potential at the ends of the cable. As shown in Section 2.2, the electric field in the cable is the same as the electric field at the seafloor along the cable route. This electric field is also applied to a transmission line model of the seawater and underlying resistive layers along the cable route to calculate the earth potentials at the cable ends.

3.1. Calculating Electric Fields at the Seafloor

The relationship between the electric and magnetic fields at the surface of the Earth is dependent on the three-dimensional (3-D) conductivity structure of the Earth. However, the variation with depth is often greater than the lateral variation and reasonable calculations can be made using a one-dimensional (1-D) model of the conductivity structure. This involves representing the Earth by a series of horizontal layers with different conductivities. The relationship between the surface electric and magnetic fields is then given by the surface impedance which is calculated using recursive formulas as shown by Weaver (1994), Boteler and Pirjola (2019). For the

seafloor calculations the changing conductivity structure along the cable route is taken into account by using different 1-D models for different cable sections (see Section 4.1). This takes into account the gross conductivity changes along the cable route.

However, we do not have measurements of the magnetic field at the seafloor, and we need to determine the relationship between the seafloor fields and the magnetic fields at the sea surface. To do this it is necessary to take into account the attenuation of the fields in the seawater above the seafloor. This has been done by Boteler and Pirjola (2003) who obtain, for an ocean of depth d , relationships between the seafloor electric field $E_S(d)$, and seafloor magnetic field $B_S(d)$, and the surface magnetic field, B_0 :

$$\frac{E_S(d)}{B_0} = \frac{Z}{\mu_0} \frac{2}{\left(1 + \frac{Z}{Z_d}\right)e^{kd} - \left(1 - \frac{Z}{Z_d}\right)e^{-kd}} \quad (13)$$

$$\frac{B_S(d)}{B_0} = \frac{Z}{Z_d} \frac{2}{\left(1 + \frac{Z}{Z_d}\right)e^{kd} - \left(1 - \frac{Z}{Z_d}\right)e^{-kd}} \quad (14)$$

Where $k = \sqrt{i2\pi f \mu_0 \sigma_S}$ and $Z = \sqrt{\frac{i2\pi f \mu_0}{\sigma_S}}$ are the propagation constant and characteristic impedance of the seawater with conductivity, $\sigma_S = 4 \text{ Sm}^{-1}$ and $Z_d = \mu_0 \frac{E_S(d)}{B_S(d)}$ is the surface impedance at the seafloor determined from a 1-D conductivity model for the subsea region using the recursive formulas of Weaver (1994) and Boteler and Pirjola (2019).

The seafloor electric field can be calculated directly from Equation 13, or with the relationship $E_S(d) = \frac{Z_d}{\mu_0} B_S(d)$, combined with the calculation of the magnetic field at the seafloor Equation 14 as done by Goto (2015). It will be seen that the two approaches are equivalent.

Python routines for calculating the seafloor electric fields are given by Chakraborty et al. (2022). SCUBAS, which stands for Submarine Cable Upset By Auroral Streams, is a cutting-edge and open-source computational model developed using the Python programming language. The SCUBAS model is specifically designed to accurately estimate the induced voltage experienced by submarine cables in the presence of geomagnetic disturbances.

3.2. Calculation of Earth Potentials at the Cable Ends

The currents induced in the ocean and the land give rise to earth potentials at the ends of the cable as explained in Section 2.3. To calculate the Earth potentials, we use the generalized thin-sheet modeling approach of Ranganayaki and Madden (1980). This represents the surface and crustal layers by an anisotropic double layer made up of a conductive layer on top with an integrated conductivity given by the product of the conductivity and the thickness of the top layer, and a resistive layer on the bottom with integrated resistivity given by the product of the resistivity and the thickness of the bottom layer.

A new efficient method for generalized thin sheet modeling has recently been introduced by Wang et al. (2023). This shows there is an equivalence between the generalized thin sheet equations and the equations developed using distributed-source transmission line theory. The transmission line model has a series impedance, Z , given by the combined conductance of the seawater and sedimentary layer and a parallel admittance, Y , given by the resistance through the crustal and mantle lithosphere resistive layers. The series impedance and parallel admittance are used to give the key parameters for the transmission line: the propagation constant, $\gamma = \sqrt{ZY}$ and the characteristic impedance, $Z_0 = \sqrt{Z/Y}$. These are dependent on the seawater depth and subsea conductivity structure in each section of the cable route. The effect of the boundary with the land at each end of the cable is included by using “active terminations” to the transmission line model as described in Boteler et al. (2023). Each transmission line section is converted to an equivalent-pi circuit, and these are combined into an admittance network. The potentials at the junctions of different sections are calculated by inversion of the admittance matrix combined with the electric fields in each section as shown by Boteler et al. (2023). The potentials within each section are then given by:

$$U_{i,k}(x) = \frac{U_k[e^{\gamma x} - e^{-\gamma x}] + U_i[e^{\gamma(L-x)} - e^{-\gamma(L-x)}]}{e^{\gamma L} - e^{-\gamma L}} \quad (15)$$

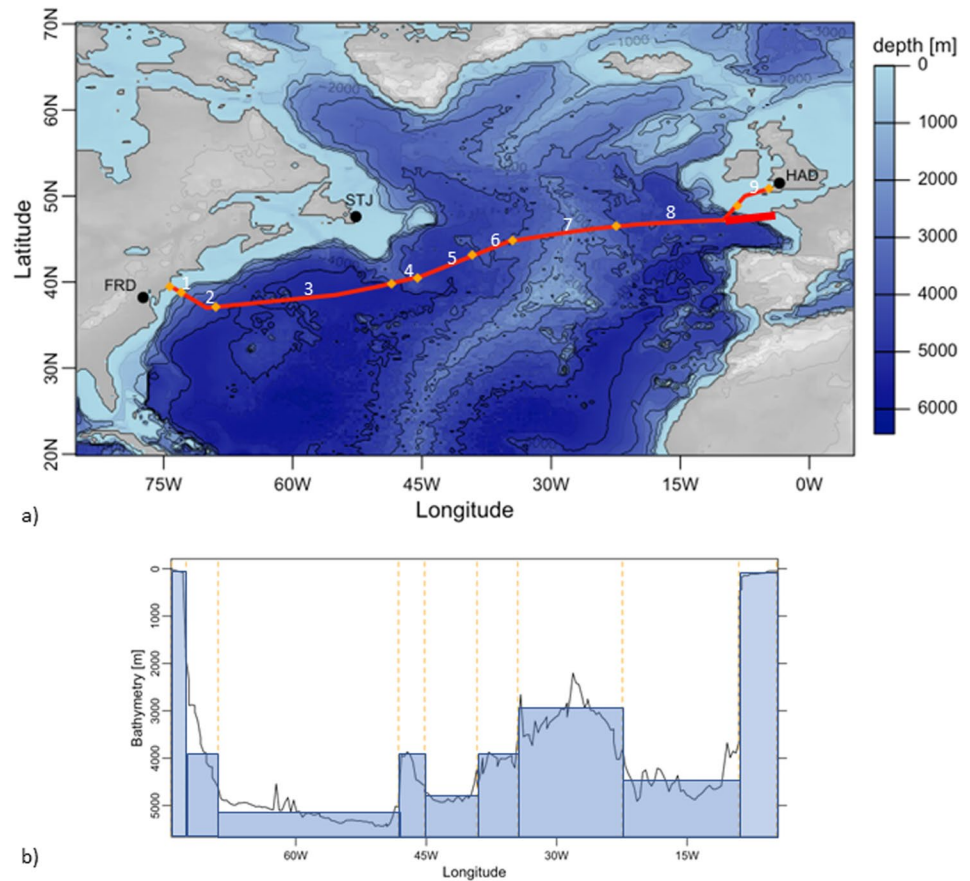


Figure 4. (a) Route of the TAT-8 submarine cable across the Atlantic. The white numbers correspond to the cable sections described in Table 1. Also shown are the locations of the Fredericksburg (FRD), St Johns (STJ), and Hartland (HAD) magnetic observatories. (b) Depth profile of the cable route. Blue blocks show the approximation of the seafloor by flat sections used in the electric field calculations.

where: U_i , and U_k , are the potentials at nodes i and k , γ is the propagation constant, L is the length of the section, and x is the distance along the section.

The important parameters obtained from these transmission line calculations are the earth potentials, U_A and U_B , at the ends of the cable.

4. Calculations for the TAT-8 Cable for 13 and 14 March 1989

To illustrate the use of the above formulas we make calculations of the voltages experienced by the first fiber-optic trans-Atlantic submarine cable, TAT-8, during the March 1989 magnetic storm. The TAT-8 cable spans a distance of 6,300 km from Tuckerton, US (39.6°N, 74.33°W) to a branching point off the coast of France from which there are connections to Widemouth Bay, UK (50.79°N, 4.55°W) and Penmarc'h, France (47.8°N, 4.34°W) as shown in Figure 4a. Power for the cable is provided by constant voltage sources at the UK and French ends and a constant current power feed at Tuckerton. By monitoring the changes in the output of the power feed equipment at Tuckerton it was possible to obtain measurements of the voltages induced in the cable (Medford et al., 1989).

The depth profile of the seafloor along the cable route from the US to the UK is shown in Figure 4b. For calculations of the electric field on the seafloor, we do not attempt to follow every change in depth along the seafloor. Instead, we approximate the seafloor by a series of sections with a flat seafloor as shown by the blue blocks in Figure 4b. The edges of the blocks are shown by the yellow marks on the cable route shown in Figure 4a.

To start the electric field calculations, we need to know the magnetic field variations along the cable route. We do not have magnetic measurements over the ocean, but we can use data from magnetic observatories near the ends of the cable: Fredericksburg (FRD) at the western end and Hartland (HAD) at the eastern end. For the middle of

Table 1
Characteristics of the Sections of the Cable Route That Are Shown in Figure 4, Together With the Earth Model and Magnetic Observatory Used for Calculating the Seafloor Electric Fields in Each Section

Section	Western edge of section	Eastern edge of section	Depth (m)	Earth model	Magnetic observatory
1	39.6°N, 74.33°W	38.79°N, 72.62°W	100	CS-W	FRD
2	38.79°N, 72.62°W	37.11°N, 68.94°W	4,000	DO-1	FRD
3	37.11°N, 68.94°W	39.80°N, 48.20°W	5,200	DO-2	STJ
4	39.80°N, 48.20°W	40.81°N, 45.19°W	4,000	DO-3	STJ
5	40.81°N, 45.19°W	43.15°N, 39.16°W	4,800	DO-4	STJ
6	43.15°N, 39.16°W	44.83°N, 34.48°W	4,000	DO-5	STJ
7	44.83°N, 34.48°W	46.51°N, 22.43°W	3,000	MAR	STJ
8	46.51°N, 22.43°W	47.85°N, 9.05°W	4,500	DO-6	HAD
9	47.85°N, 9.05°W	50.79°N, 4.55°W	100	CS-E	HAD

the cable, we use magnetic data from St Johns (STJ) magnetic observatory in Newfoundland to the north of the cable route (see Figure 4a). The observatories chosen for use with each cable section are shown in Table 1 and correspond to the observatory closest to the middle of each section. The magnetic field variations recorded at these three observatories on 13 and 14 March 1989, are shown in Figure 5.

The seafloor sections are described in Table 1 which shows the sea depth for each section and the latitude and longitude of the section edges along the cable route as well as the Earth model used for the underlying conductivity structure and the magnetic observatory used for calculating electric fields.

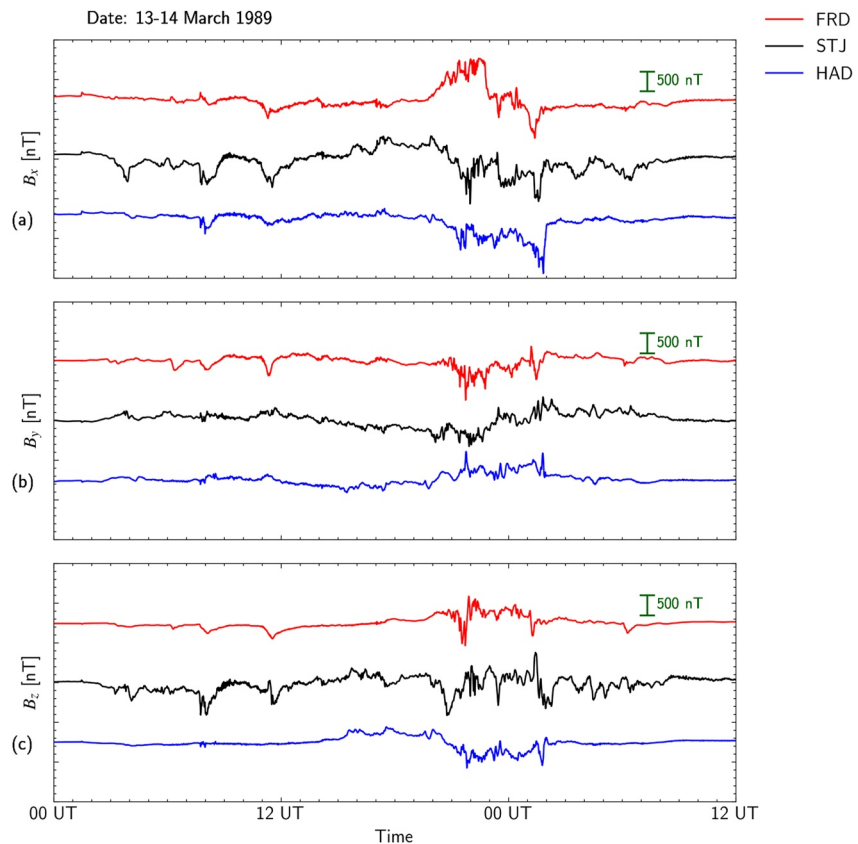


Figure 5. Measured magnetic field variations at Fredericksberg (FRD), St John's (STJ) and Hartland (HAD) near the west end, middle, and east end of the cable route during the magnetic disturbance of 13 and 14 March 1989. (a) X component, (b) Y component, (c) Z component.

Table 2
Seawater Depths and Subsea Earth Conductivity Models for the Sections of the TAT-8 Submarine Cable Route That Are Shown in Figure 4

Layer	Resistivity (ohm-m)	Layer thickness (km)								
		CS-W	DO-1	DO-2	DO-3	DO-4	DO-5	MAR	DO-6	CS-E
Seawater	0.3	0.1	4	5.2	4	4.8	4	3	4.5	0.1
Sediments	3	8	4	2	2	1	0.5	0	1.5	3
Crust	3,000	15	10	10	10	10	10	10	10	20
Mantle Lithosphere	1000	150	145	140	140	70	60	25	70	120
Upper Mantle	100	236.9	247	252.8	254	324.2	335.5	372	324	266.9
Transition Zone	10	250	250	250	250	250	250	250	250	250
Lower Mantle	1	340	340	340	340	340	340	340	340	340

4.1. Transfer Functions for the North Atlantic

To calculate the electric fields produced at the seafloor by the magnetic field variations shown in Figure 5 we need to know the transfer function between the seafloor electric fields and the surface magnetic fields. This is dependent on the depth and conductivity of the seawater and the surface impedance of the Earth underlying the seafloor. To take into account lateral changes in conductivity a simplified approximation is to use a “piecewise” approach with different one-dimensional (1-D) Earth models used for different geologic zones (Marti et al., 2014).

The sea depths along the cable route are derived from the ETOPO1 model (Amante & Eakins, 2009). The subsea Earth conductivity models are based on the LITHO1.0 model (Pasyanos et al., 2014). These models (Table 2) show the shallow seawater depth on the continental shelf (CS) at the western and eastern ends of the cable. Between those sections are deep ocean (DO) regions with similar properties except for the shallower section of the Mid-Atlantic Ridge (MAR) where the upwelling magma creates a higher conductivity region in the mantle lithosphere.

The earth models shown in Table 2 were used to calculate the seafloor impedance Z_d for the different sections along the cable route. Then Equation 13 was used with the appropriate depth, d , of seawater and seawater conductivity $\sigma = 4$ S/m to determine the transfer function T_x between the seafloor electric field and the surface magnetic field for each section. These transfer functions (Figure 6) show that the transfer function amplitude decreases with increasing depth of the seafloor; indicating that the deeper parts of the ocean will experience smaller electric fields, and these are noticeably smaller than the electric field at the seafloor of the continental shelf.

4.2. Electric Field Calculations for 13 and 14 March 1989

The transfer function in Equation 13 represents the relationship between a right-handed pair of orthogonal seafloor electric fields and a surface magnetic field across the whole frequency range considered. Thus, it can be used to relate the northward component, E^N , and eastward component, E^E , of the seafloor electric field to the eastward component, B^E , and northward component, B^N , of the surface magnetic field, respectively.

$$\begin{aligned} E^N(f) &= T_x(f)B^E(f) \\ -E^E(f) &= T_x(f)B^N(f) \end{aligned} \quad (16)$$

These equations represent the relationship in the frequency domain.

To calculate the variations of the electric field in the time domain we start with the time series of the northward and eastward components of the magnetic field recorded at the chosen magnetic observatories and take the Fourier transform of each part to give the magnetic field spectra in the frequency domain. Each magnetic field frequency component is multiplied by the corresponding transfer function (complex) value to give the frequency components of the electric field spectra. An inverse Fourier transform of these spectra then gives the components of the electric field in the time domain

$$E^N(t) = \mathcal{F}^{-1}[T_x(f) \mathcal{F}\{B^E(t)\}] \quad (17)$$

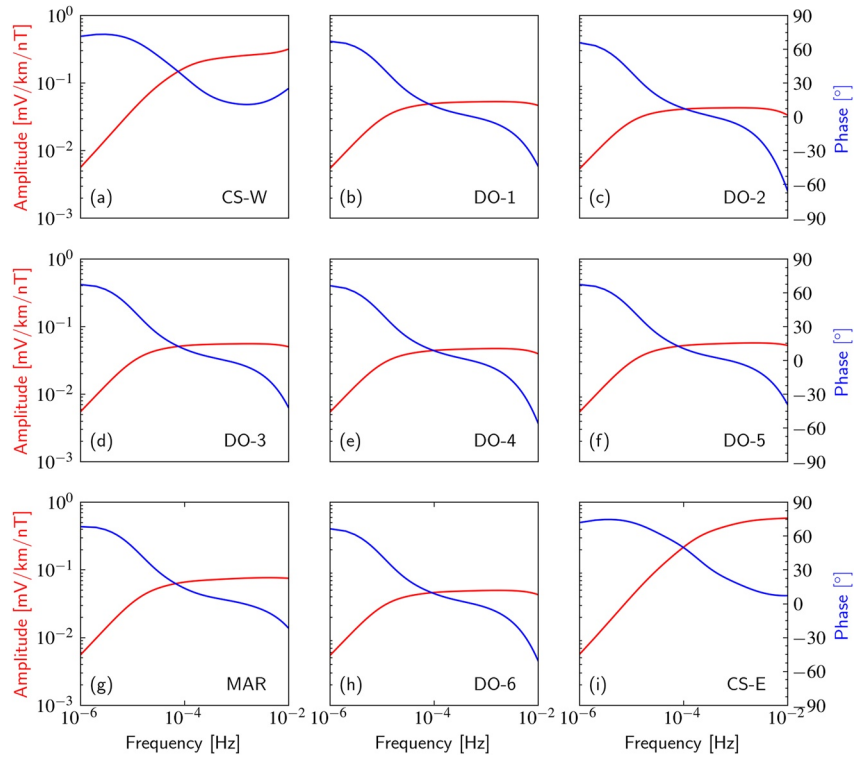


Figure 6. Transfer functions relating the seafloor electric field to the surface magnetic field, calculated using the subsea earth models shown in Table 2.

$$-E^E(t) = F^{-1}[T_X(f) F\{B^N(t)\}] \quad (18)$$

This process is repeated for each section, i , of the cable route using the appropriate transfer function, T_X , and data from the closest magnetic observatory as shown in Table 1 to give the electric fields in each section shown in Figure 7.

The induced emf, \mathcal{E}_i , in each cable section is then given by

$$\mathcal{E}_i(t) = E_i^N(t) L_i^N + E_i^E(t) L_i^E \quad (19)$$

where the north-south length L^N and east-west length L^E are calculated from the latitude and longitude of the ends of the section (Table 1) using the Formulas A3 and A7 for the WGS84 Geodetic model of the Earth as described in the Appendix of Horton et al. (2012). These are shown in Figure 8.

4.3. Calculation of TAT-8 Voltages for 13 and 14 March 1989

The voltage experienced by a submarine cable is comprised of two parts: the induced electromotive force (emf) induced by the magnetic field variations directly into the cable and the potential difference between the ends of the cable as shown in Equation 12.

To obtain the total induced emf, \mathcal{E}_C , along the cable route, we sum the emfs from each section

$$\mathcal{E}_C = \sum_{i=1}^9 \mathcal{E}_i(t) \quad (20)$$

To obtain the Earth potentials at the cable ends, we use DSTL modeling of the Ocean/Earth conductivity structure along the cable route as described by Boteler et al. (2023). The SCUBAS parameters for the route of the TAT-8 cable are shown in Table 3. The effect of induction in the land at either end can be included in the modeling by adding active terminations as described by Boteler et al. (2023) (see the Supporting Information S1).

Applying Equation 12 to the TAT-8 cable across the North Atlantic, we get

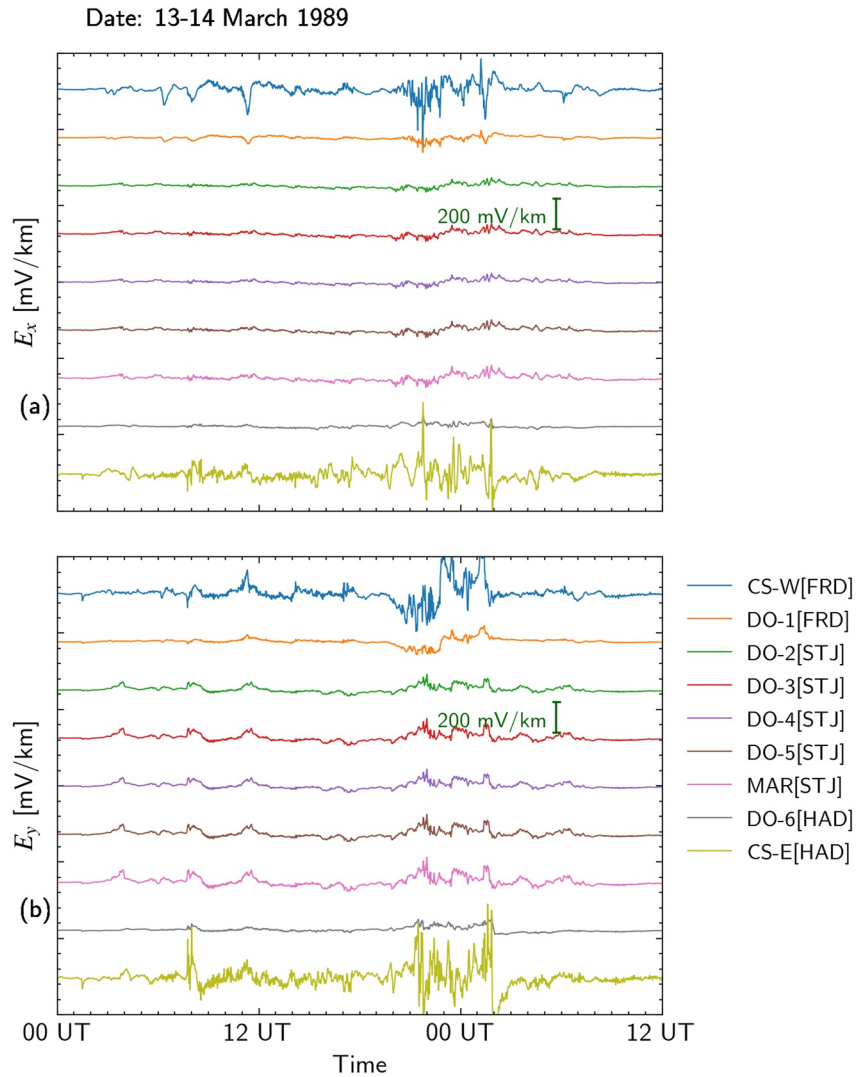


Figure 7. Seafloor electric fields during the magnetic storm of 13 and 14 March 1989 calculated for the 9 sections of the TAT-8 cable route across the North Atlantic using the magnetic observatory data and earth models as noted in Table 1.

$$V_{\text{TAT-8}} = \mathcal{E}_C + U_W - U_E \quad (21)$$

Where: \mathcal{E}_C is the sum of the induced emfs in the cable sections given by Equation 20,

U_W is the Earth potential at the west end of the TAT-8 cable,

U_E is the Earth potential at the east end of the TAT-8 cable.

The terms on the right of Equation 21 as well as the resulting voltage variations for the TAT-8 cable during the 13 and 14 March 1989, geomagnetic disturbance are shown in Figure 9.

4.4. Comparison With Recordings on the TAT-8 Cable

Recordings of TAT-8 Power feed equipment (PFE) voltage variations during the 13 and 14 March 1989 magnetic disturbance are shown in the paper by Medford et al. (1989). They also give a table of the largest PFE voltage excursions measured on the TAT-8 cable during the March 1989 event; these are reproduced in Table 4, rearranged to be in chronological order.

The PFE drives an electric current from North America to Europe along the cable (Calvo et al., 1988). Thus, a westward geomagnetically induced electric field will oppose the normal current along the cable causing an

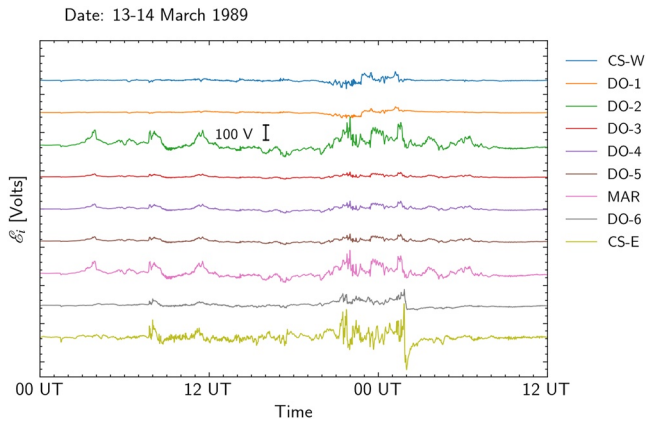


Figure 8. Induced emfs produced during the magnetic storm of 13 and 14 March 1989, calculated from Equation 19 for each section of the TAT-8 cable route using the magnetic observatory data and Earth models as shown in Table 1.

increase in the PFE voltage to compensate and maintain a constant current flow through the cable. Conversely, an eastward geomagnetically induced electric field will tend to increase the current in the cable causing the PFE to reduce its voltage to keep the cable current at a constant value.

The calculated cable voltage variations shown in Figure 9 are used to determine the calculated values for the same parts of the event as used by Medford et al. (1989). These are shown in the last column of Table 4. The similarity of the calculated values to the measured values reported by Medford et al. (column 3 of Table 4) provides support for the method of calculation presented here.

5. Discussion

The example calculations for the TAT-8 submarine cable illustrate some of the factors that have an influence on the voltage experienced by the cable. These range from the spatial characteristics of the magnetic field variations to the frequency content seen at different parts of the cable route and the tendency for the earth potentials at the ends of the cable to reduce the effect of the induced emf in the cable.

The TAT-8 cable spans 6,300 km, covering 5 hr in local time, so it can be expected that a lot of the time the magnetic field variations at opposite ends of the cable will be significantly different. For example, in the evening of March 13, the Fredericksburg magnetic observatory at the western end of the cable is showing a positive variation in B_x produced by an eastward electrojet in the afternoon sector, whereas Hartland magnetic observatory at the eastern end of the cable is showing a negative variation in B_x produced by a westward electrojet in the midnight sector (Figure 10a). [This was also identified by Lanzerotti et al. (2001).] In this case, even though the magnetic field variations are significant, they produce electric fields at opposite ends of the cable that tend to cancel each other, so the overall impact on the cable is reduced.

There are times, however, when a similar magnetic disturbance is seen across the whole length of the cable. Figure 5 shows that this occurs at 01.30 UT on March 14 and indicates that a westward electrojet extended from Europe to North America (Figure 10b). In this case, an eastward electric field is induced along the whole length of the cable and produces a larger cable voltage than during the earlier interval examined above. It should be noted that 01.30 UT on March 14 is the time when the recordings on the TAT-8 cable showed the largest voltage excursion (see Table 4). The electric fields produced in different sections of the cable are also influenced by the seawater depth in each section with the deeper sections experiencing much more attenuation of the fields than the shallow sections. The first indication of this is given in Figure 6 which shows that the seafloor/surface transfer functions for the two continental shelf sections have higher values than those for the deep ocean sections. The effect of this is seen in Figure 7 which shows that the seafloor electric fields in the continental shelf sections are larger than those in the deep ocean sections. The overall impact of this on the voltages experienced by the cable depends on the relative contributions from the continental shelf and deep ocean sections.

Earth potentials at the ends of the cable also contribute to the overall voltage experienced by the cable power feed equipment. At times when the electric field is directed eastward in the sea and in the cable, there will be a negative Earth potential at the western end of the cable and a positive Earth potential at the eastern end. This potential difference between the ends of the cable acts against the eastward electric field and reduces the overall voltage experienced by the cable.

This paper has examined the various factors that influence the voltages experienced by submarine cable power feed equipment during geomagnetic disturbances. The calculation procedure that has been developed takes account of the changing depth of seawater along the cable route as well as changes to

Table 3
Transmission Line (Thin Sheet) Model of the Route of the TAT-8 Submarine Cable

Region	Length (km)	Z (Ω/km)	Y (S/km)	γ (1/km)	Z_0 (Ω)	Adj dist (km)
Sea (west)	105	0.333	$5.13 \cdot 10^{-6}$	$13.1 \cdot 10^{-4}$	255	763
Ocean 1	231	$6.82 \cdot 10^{-2}$	$5.71 \cdot 10^{-6}$	$6.24 \cdot 10^{-4}$	109	1603
Ocean 2	1243	$5.56 \cdot 10^{-2}$	$5.88 \cdot 10^{-6}$	$5.72 \cdot 10^{-4}$	97.2	1748
Ocean 3	256	$7.14 \cdot 10^{-2}$	$5.88 \cdot 10^{-6}$	$6.48 \cdot 10^{-4}$	110	1543
Ocean 4	561	$6.12 \cdot 10^{-2}$	$10.0 \cdot 10^{-6}$	$7.82 \cdot 10^{-4}$	78.2	1279
Ocean 5	457	$7.41 \cdot 10^{-2}$	$11.1 \cdot 10^{-6}$	$9.07 \cdot 10^{-4}$	81.7	1103
Ocean 6	1194	$10.0 \cdot 10^{-2}$	$18.2 \cdot 10^{-6}$	$13.5 \cdot 10^{-4}$	74.2	741
Ocean 7	1441	$6.45 \cdot 10^{-2}$	$10.0 \cdot 10^{-6}$	$8.03 \cdot 10^{-4}$	80.3	1245
Sea (east)	594	0.75	$5.56 \cdot 10^{-6}$	$20.4 \cdot 10^{-4}$	367	490

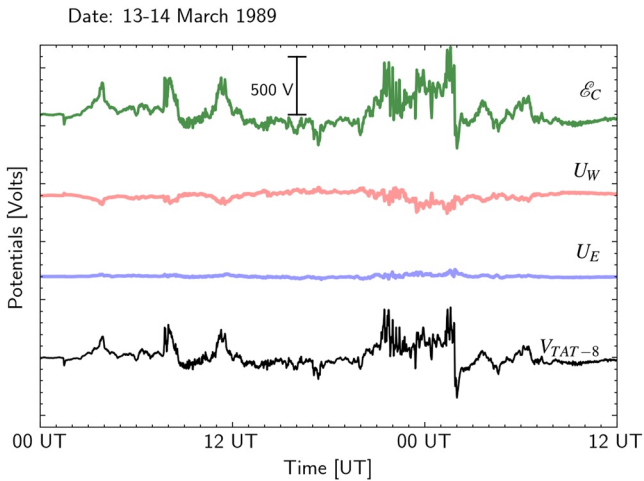


Figure 9. Final calculated result for voltage produced in the TAT-8 cable by the geomagnetic disturbance on 13 and 14 March 1989, using magnetic observatory data and earth models as shown in Table 1, and the transmission line model shown in Table 3. The figure shows all the terms in Equation 21, from top to bottom: 1) Total induced emf along the cable, \mathcal{E}_C ; 2) Earth potential at west end, U_W ; 3) Earth potential at east end, U_E ; 4) Total voltage experienced by the cable, V_{TAT-8} .

the earth conductivity structure below the seafloor to calculate the induced emf experienced by the cable. It also models the induction in the seawater and the land at either end to determine the Earth potentials at the ends of the cable. Spatial structure in the geomagnetic disturbance is taken into account by using magnetic data from observatories at either end of the cable; for the TAT-8 cable we have also been able to use magnetic data from the St John's magnetic observatory as an approximation to the magnetic disturbance in the middle of the cable route, but such an option will not necessarily be possible for other submarine cables.

The results obtained from the calculations give cable voltage values that are very similar to those measured on the TAT-8 cable during the March 1989 storm (Medford et al., 1989). This is encouraging but may exaggerate the results that can generally be achieved from such modeling. Even if the calculation of the electric fields experienced by the cable is refined by the use of more sophisticated modeling techniques, a fundamental limitation will always be the lack of magnetic data from along the cable route to use as input for the modeling. This can also be a limitation for studies of geomagnetic effects on land-based systems; but the installation of magnetometers is much easier on land than on the seafloor. As with studies of geomagnetic induction on land-based systems, calculations can also be made using interpolation techniques to obtain the best estimate of the magnetic disturbances along the cable route. Future work will also examine geomagnetic induction produced by modeled ionospheric and magnetospheric current sources.

The agreement between the modeling results and the measurements reported by Medford et al. (1989) may be because their study primarily focussed on the largest disturbances on the cable. Because the cable will experience the largest voltages when the electric fields are similar along the whole cable, this naturally selects out those parts of the disturbance where the magnetic field variations are fairly uniform across the Atlantic. The smaller event considered, the SSC on March 13, also produces a fairly uniform magnetic field variation along the whole cable route. The significance of this is that the more uniform the disturbance, the better chance that the magnetic disturbances recorded on land will be representative of the magnetic disturbances out over the ocean. For times when the cable voltage is smaller, there might be more spatial structure in the magnetic disturbance so that the electric fields produced in different parts of the cable tend to cancel each other. In such situations, because of the spatial structure, the recordings at the magnetic observatories on land will likely be less reliable indicators of the magnetic field variations out over the ocean. However, the fact that the calculation works best for large-scale disturbances is not a bad thing. These disturbances are the ones that will produce the largest voltages on the cable and are therefore the events of most concern.

Submarine cables carry over 95% of international internet traffic and have become a vital critical infrastructure for modern societies. Consequently, it is important to evaluate any natural hazards that could potentially interfere with their operation. This paper has shown how the voltages produced in submarine cables during geomagnetic disturbances can be modeled. In future work this modeling will be used with archived magnetic observatory data to calculate the voltages produced in trans-Atlantic cables over the last 30 years to assess the geomagnetic hazard. This will then be coupled with an analysis of the evolving vulnerability of submarine cable systems to perform an assessment of the space weather risks to submarine cables.

Table 4
Peak Voltages on the TAT-8 Cable During the March 13-14, 1989 Magnetic Disturbance Reported by Medford et al. (1989), and the Calculated Cable Voltages

“Event”	Measured PFE voltage excursion (V)	Calculated cable voltage variation (V)
SSC, 01.30 UT, March 13	~75	67
11.10 UT, March 13	~300	249
21.45 UT, March 13	~450	406
01.30 UT, March 14	~700	763

6. Conclusions

Submarine cables are a vital part of modern communications infrastructure. They now use optical fibers to carry the signals but there is a copper conductor in the cable to supply power to the repeaters. It is the power feed to the cable that is potentially affected by geomagnetic disturbances, as shown by the recordings from the TAT-8 trans-Atlantic cable during the March 1989 geomagnetic disturbance when voltage variations up to 700 V were measured.

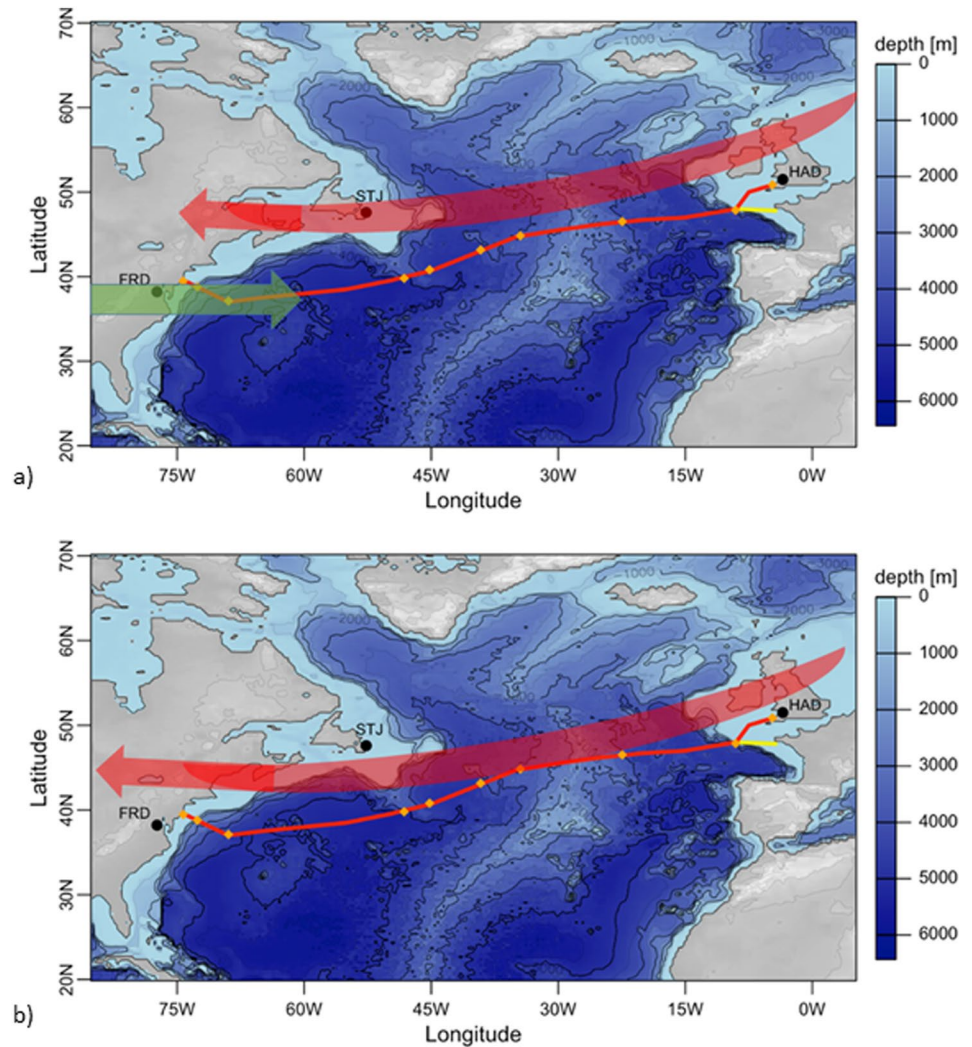


Figure 10. Electrojet positions estimated from the magnetic field variations in Figure 4 (a) For the disturbance at 21.45 UT on March 13, (b) For the disturbance at 01.30 UT on March 14.

A new calculation method using magnetic observatory data and models of the Ocean/Earth conductivity structure has been used to calculate both the geomagnetically induced emf in the cable, \mathcal{E}_C and the Earth potentials U_A and U_B at ends A and B of the cable. The voltage experienced by the cable, V_C , is then:

$$V_C = \mathcal{E}_C + U_A - U_B \quad (22)$$

Example calculations for the TAT-8 trans-Atlantic cable closely match the peak values measured on the cable during the March 1989 geomagnetic disturbance, providing confidence in the new method.

The new method considers that the primary effect of geomagnetic induction for submarine cables is the production of an induced electromotive force (emf) in the cable itself. Induction also occurs in the seawater and the land at either end of the cable driving different currents in each; current continuity across the conductivity boundary at each coast is achieved by charge accumulation which changes the earth potential at each end of the cable.

Larger seafloor electric fields were produced in the shallow continental shelf sections of the cable route compared to those in the deep ocean sections. For the TAT-8 cable, the continental shelf sections represented 11% of the cable route but contributed, on average, 21% of the electric field integrated along the cable route. This shows that the continental shelf sections have higher electric fields per unit length, but the much greater length of the deep ocean sections means that they contribute most to the total emf experienced by the cable.

The calculation method requires knowledge of the geomagnetic field variations along the cable route. For the TAT-8 cable, magnetic observatories at each end of the cable and a site to the north of the middle of the cable provide a reasonable source of data for large-scale magnetic disturbances affecting the cable. Other cables may not have such a fortuitous placement of magnetic observatories. However, the modeling could also be used with synthetic magnetic variations as input, allowing the impact of different levels of geomagnetic activity on submarine cables to be assessed.

Data Availability Statement

The data sets used in this study are synthetically produced inside the code and can be found in the Zenodo repository (Chakraborty, 2023). The crust and lithospheric model of the Earth LITHO1.0 model (Pasyanos et al., 2014) is available on IRIS DMC Data Products website (Trabant et al., 2012). The computational model, SCUBAS: Submarine Cables Upset by Auroral Streams., is developed using Python to compute geomagnetic induction effect on submarine cables (Chakraborty, 2022). A pip installer is also available to install the model in any python environment. Example codes are also available to describe the parameters and illustrate the use of SCUBAS (Chakraborty et al., 2022). Please refer to the website for detailed documentation on SCUBAS. The majority of analysis and visualization was completed with the help of free, open-source software tools such as matplotlib (Hunter, 2007), IPython (Perez & Granger, 2007), pandas (McKinney, 2010), and others (e.g., Millman & Aivazis, 2011). Our code is published in Zenodo repository (Chakraborty & Shi, 2023).

Acknowledgments

We thank Lidia Nikitina and Laurel Sinclair for useful comments on the manuscript. DHB was supported by Natural Resources Canada. SC and MDH were supported by NASA awards 80NSSC19K0907 and 80NSSC21K1677. XS was supported by NASA awards 80NSSC19K0907, 80NSSC21K1677, and the NASA DRIVE Science Center for Geospace Storms (CGS) under award 80NSSC22M0163. SC and XS also thank the National Science Foundation for support under Grant AGS-1935110. The magnetic observatory data for the March 1989 storm are available from the respective observatory operators: Fredericksburg—United States Geological Survey, St Johns—Natural Resources Canada, Hartland—British Geological Survey, or from the World Data Centre for Geomagnetism, Kyoto. NRCan contribution number: 20220386.

References

- Amante, C., & Eakins, B. W. (2009). *ETOPO1 1 arc-minute global relief model: Procedures, data sources and analysis* (p. 19). NOAA Technical Memorandum NESDIS NGDC-24. Retrieved from <https://www.ngdc.noaa.gov/mgg/global/relief/ETOPO1/docs/ETOPO1.pdf>
- Anderson, C. W. (1978). Magnetic storms and cable communications. In C. F. Kennel, L. J. Lanzerotti, & E. N. Parker (Eds.), *Solar system plasma physics*. North-Holland.
- Anderson, C. W., III., Lanzerotti, L. J., & MacLennan, C. G. (1974). Outage of the L4 system and the geomagnetic disturbances of 4 August 1972. *Bell System Technical Journal*, 53(9), 1817–1837. <https://doi.org/10.1002/j.1538-7305.1974.tb02817.x>
- Boteler, D. H. (2006). The super storms of August/September 1859 and their effects on the telegraph system. *Advances in Space Research*, 38(2), 159–172. <https://doi.org/10.1016/j.asr.2006.01.013>
- Boteler, D. H., Chakraborty, S., Xueling Shi, X., Hartinger, M. D., & Wang, X. (2023). Transmission line modelling of geomagnetic induction in the ocean/Earth conductivity structure. *International Journal of Geosciences*, 14(08), 767–791. <https://doi.org/10.4236/ijg.2023.148041>
- Boteler, D. H., & Pirjola, R. J. (1997). Nature of the geoelectric field associated with GIC in long conductors such as power systems, pipelines, and phone cables. In *Proceedings of second international symposium on electromagnetic compatibility, Beijing, May 21–23, 1997*. Beijing University of Posts and Telecommunications.
- Boteler, D. H., & Pirjola, R. J. (1998). Modelling geomagnetically induced currents produced by realistic and uniform electric fields. *IEEE Transactions on Power Delivery*, 13(4), 1303–1308. <https://doi.org/10.1109/61.714500>
- Boteler, D. H., & Pirjola, R. J. (2003). The magnetic and electric fields produced in the sea during geomagnetic disturbances. *Pure and Applied Geophysics*, 160(9), 1695–1716. <https://doi.org/10.1007/s00024-003-2372-6>
- Boteler, D. H., & Pirjola, R. J. (2017). Modeling geomagnetically induced currents. *Space Weather*, 15(1), 258–276. <https://doi.org/10.1002/2016SW001499>
- Boteler, D. H., & Pirjola, R. J. (2019). Numerical calculation of geoelectric fields that affect critical infrastructure. *International Journal of Geosciences*, 10, 930–949. <https://doi.org/10.4236/ijg.2019.1010053>
- Boteler, D. H., Pirjola, R. J., & Nevanlinna, H. (1998). The effects of geomagnetic disturbances on electrical systems at the Earth's surface. *Advances in Space Research*, 22(1), 17–27. [https://doi.org/10.1016/s0273-1177\(97\)01096-x](https://doi.org/10.1016/s0273-1177(97)01096-x)
- Bullard, E. C., & Parker, R. L. (1970). Electromagnetic induction in the oceans. In A. E. Maxwell (Ed.), *The sea, Chapter 18* (Vol. 4, pp. 695–730). Wiley-Interscience.
- Burbank, J. E. (1905). Earth-currents and a proposed method for their investigation. *Terrestrial Magnetism and Atmospheric Electricity*, 10(1), 23–49. <https://doi.org/10.1029/te010i001p00023>
- Cagniard, L. (1953). Principe de la method magneto-tellurique. *Annales Geophysicae*, 9(2), 95–125.
- Calvo, O. A., Hamilton, B. H., Layendecker, R. A., Slak, W. M., & Zweig, W. L. (1988). Power feed equipment for the SL undersea light-wave cable. In *10th international telecommunications energy conference, San Diego, CA, USA, 1988* (pp. 194–200). <https://doi.org/10.1109/INTLEC.1988.22349>
- Chakraborty (2023). shibaji7/submarine_cable_modeling: Codebase for space weather paper (V2.0-SW). *Zenodo*. <https://doi.org/10.5281/zenodo.10064385>
- Chakraborty, S. (2022). shibaji7/submarine_cable_modeling: Geomagnetic Induction in Submarine Cables. <https://doi.org/10.5281/zenodo.7055321>
- Chakraborty, S., Boteler, D. H., Xueling Shi, X., Murphy, B. S., Hartinger, M. D., Wang, X., et al. (2022). Modeling geomagnetic induction in submarine cables. *Frontiers in Physics*, 10, 1022475. <https://doi.org/10.3389/fphy.2022.1022475>
- Chakraborty, S., & Shi, X. (2023). shibaji7/SCUBAS: Transmission line modeling (TLM-0.1.3). *Zenodo*. <https://doi.org/10.5281/zenodo.7778688>
- Cox, C. S., Filloux, J. H., & Larsen, J. C. (1970). Electromagnetic studies of ocean currents and electrical conductivity below the ocean floor. In A. E. Maxwell (Ed.), *The sea, Chapter 17* (Vol. 4, pp. 637–694). Wiley-Interscience.
- Goto, T. (2015). Numerical studies of geomagnetically induced electric field on seafloor and near coastal zones incorporated with heterogeneous conductivity distributions. *Earth Planets and Space*, 67(1), 193. <https://doi.org/10.1186/s40623-015-0356-2>

- Horton, R., Boteler, D. H., Overbye, T. J., Pirjola, R. J., & Dugan, R. (2012). A test case for the calculation of geomagnetically induced currents. *IEEE Transactions on Power Delivery*, 27(4), 2368–2373. <https://doi.org/10.1109/tpwrd.2012.2206407>
- Hunter, J. D. (2007). Matplotlib: A 2D graphics environment. *Computing in Science & Engineering*, 9(3), 90–95. <https://doi.org/10.1109/MCSE.2007.55>
- Lanzerotti, L. J., & Gregori, G. P. (1986). Telluric currents: The natural environment and interactions with man-made systems. In *The Earth's electrical environment* (pp. 232–257). The National Academies Press.
- Lanzerotti, L. J., Medford, L. V., MacLennan, C. G., Kraus, J. S., Kappenman, J., & Radasky, W. (2001). Trans-Atlantic geopotentials during the July 2000 solar event and geomagnetic storm. *Solar Physics*, 204(1/2), 351–359. <https://doi.org/10.1023/a:1014289410205>
- Marti, L., Yiu, C., Rezaei-Zare, A., & Boteler, D. (2014). Simulation of geomagnetically induced currents with piecewise layered-Earth models. *IEEE Transactions on Power Delivery*, 29(4), 1886–1893. <https://doi.org/10.1109/tpwrd.2014.2317851>
- McKinney, W. (2010). Data structures for statistical computing in Python. In S. van derWalt & J. Millman (Eds.), *Proceedings of the 9th Python in science conference* (pp. 56–61). <https://doi.org/10.25080/Majora-92bf1922-012>
- Medford, L. V., Lanzerotti, L. J., Kraus, J. S., & MacLennan, C. G. (1989). Transatlantic earth potential variations during the March 1989 magnetic storms. *Geophysical Research Letters*, 16(10), 1145–1148. <https://doi.org/10.1029/gl016i010p01145>
- Medford, L. V., Meloni, A., Lanzerotti, L. J., & Gregori, G. P. (1981). Geomagnetic induction on a transatlantic communications cable. *Nature*, 290(5805), 392–393. <https://doi.org/10.1038/290392a0>
- Millman, K. J., & Aivazis, M. (2011). Python for scientists and engineers. *Computing in Science & Engineering*, 13(2), 9–12. <https://doi.org/10.1109/MCSE.2011.36>
- Pasyanos, M. E., Masters, T. G., Laske, G., & Ma, Z. (2014). Litho1.0: An updated crust and lithospheric model of the earth. *Journal of Geophysical Research: Solid Earth*, 119(3), 2153–2173. <https://doi.org/10.1002/2013JB010626>
- Perez, F., & Granger, B. E. (2007). Ipython: A system for interactive scientific computing. *Computing in Science & Engineering*, 9(3), 21–29. <https://doi.org/10.1109/MCSE.2007.53>
- Prescott, G. B. (1866). *History, theory and practice of the electric telegraph*. Ticknor and Fields.
- Price, A. T. (1962). The theory of the magnetotelluric methods when the source field is considered. *Journal of Geophysical Research*, 67(5), 1907–1918. <https://doi.org/10.1029/jz067i005p01907>
- Price, A. T. (1973). The theory of geomagnetic induction. *Physics of the Earth and Planetary Interiors*, 7(3), 227–233. [https://doi.org/10.1016/0031-9201\(73\)90049-6](https://doi.org/10.1016/0031-9201(73)90049-6)
- Ranganayaki, R. P., & Madden, T. R. (1980). Generalized thin sheet analysis in magnetotellurics: An extension of Price's analysis. *Geophysical Journal of the Royal Astronomical Society*, 60(3), 445–457. <https://doi.org/10.1111/j.1365-246x.1980.tb04820.x>
- Tikhonov, A. N. (1950). Determination of the electrical characteristics of deep layers of the earth's crust. *Doklady Akademii Nauk*, 73, 275.
- Trabant, C., Hutko, A. R., Bahavar, M., Karstens, R., Ahern, T., & Aster, R. (2012). Data products at the IRIS DMC: Stepping stones for research and other applications. *Seismological Research Letters*, 83(5), 846–854. <https://doi.org/10.1785/0220120032>
- Wait, J. R. (1954). On the relation between telluric currents and the earth's magnetic field. *Geophysics*, 19(2), 281–289. <https://doi.org/10.1190/1.1437994>
- Wait, J. R. (1962). Theory of magneto-telluric fields. *Journal of Research of the National Bureau of Standards*, 66D(5), 509–541. <https://doi.org/10.6028/jres.066d.052>
- Wang, X., Boteler, D. H., & Pirjola, R. (2023). Distributed-source transmission line theory for modeling the coast effect on geoelectric fields. *IEEE Transactions on Power Delivery*, 38(5), 3541–3550. <https://doi.org/10.1109/tpwrd.2023.3279462>
- Weaver, J. T. (1994). *Mathematical methods for GeoElectromagnetic induction*. Research Studies Press.
- Winckler, J. R., Peterson, L., Hoffman, R., & Arnoldy, R. (1959). Auroral X-rays, cosmic rays, and related phenomena during the storm of Feb 10–11, 1958. *Journal of Geophysical Research*, 64(6), 597–610. <https://doi.org/10.1029/jz064i006p00597>